JOURNAL OF THERMOPHYSICS AND HEAT TRANSFER
Vol. 19, No. 2, April–June 2005

Quasi-Classical Trajectory Modeling of OH Production in Direct Simulation Monte Carlo

Takashi Ozawa,* Dmitry Fedosov,* and D. A. Levin†
Pennsylvania State University, University Park, Pennsylvania 16802
and
S. F. Gimelshein‡
University of Southern California, Los Angeles, California 90089

The quasi-classical trajectory method enables one to obtain reaction probabilities and cross sections for fundamental reactions and to simulate strongly nonequilibrium flows. The formation of vibrationally hot OH for a rarefied flow about a sphere at 80- and 100-km altitudes are examined with the direct simulation Monte Carlo (DSMC) method. The main objective is to apply new chemistry models in the DSMC simulations of OH formation mechanisms in hypersonic flows at high altitudes. Using a numerically efficient parallel molecular dynamics (MD) code, we calculate the reaction cross sections and OH product rotational and vibrational distributions for two exchange reactions, $H + O_2 \rightarrow OH + O$ and $O + H_2 \rightarrow OH + H$. The reaction probabilities are then used in a DSMC computational tool to study OH production at 80- and 100-km altitudes. It is found that at 100 km the $H + O_2$ exchange reaction is the main production mechanism of OH. Approximately an order of magnitude difference is observed for the MD and total collision energy rates, and differences in the predicted vibrational OH temperature were also obtained.

Nomenclature

b	=	impact parameter
E_{int}	=	internal energy, J
E_{tr}	=	translational energy, J
J	=	rotational quantum number
k	=	Boltzmann constant
k_f	=	thermal rate constant
$p_{i,j}$	=	Cartesian momentum coordinate
Q_{rot}	=	rotational partition function
Q_{vib}	=	vibrational partition function
R_{12}	=	O–O or H–H internuclear distance
T	=	temperature
V	=	potential energy, J
v	=	vibrational quantum number
W	=	weighting factor
σ	=	reaction cross section

I. Introduction

ONE of the recent challenging topics of the direct simulation Monte Carlo (DSMC) method is the study of radiation that occurs in a hypersonic flow about reentry vehicles at high altitudes for a wide range of wavelengths from infrared to ultraviolet. The spectral radiation from high-energy rarefied gas flows provides us with a sensitive metric for the evaluation of energy exchange and chemical reaction models. The modeling of ultraviolet emissions from hypersonic bow shocks gives an important indication of the flowfield gas properties. The Bow-Shock Ultraviolet (BSUV) Flight Experiment[1] obtained spectra of OH($A^2\Sigma^+ - X^2\Pi$) UV radiation between altitudes of 80 and 100 km. The data indicate that the OH(A) species formed in rarefied, high-energy flows have internal energies much greater than that of the bulk flow. Because there are so few collisions in these flows, the spectral data may be used to test the ability of theory to model near-nascent distributions of chemically produced radiating species and energy exchange. The UV spectra of OH(A) are well defined and originate from a single excited electronic state. Under rarefied conditions, the OH(A) UV spectra are sensitive to the chemical processes involved in OH formation.

Earlier work[2] demonstrated the sensitivity of the OH spectra to variation in the vibrational temperature. It was shown that the ratio of the peak heights at 2800 Å (due to 1–0 transition) and 3100 Å (due to 0–0 transition) depends mainly on the vibrational temperature. An OH vibrational temperature in the range of 4000–7000 K was estimated from the spectral data, demonstrating that the OH vibrational temperature is significantly higher than the predicted shock-layer bulk (N_2) vibrational temperature of ~700 K for this range of altitudes. More detailed treatment of the coupling of the flow and radiation modeling has been undertaken for the OH(A) system.[3] However, this work did not lead to OH vibrational temperatures consistent with the BSUV 2.

In earlier work,[4] a detailed modeling of vibrational temperatures and distributions of OH produced by collision-induced water dissociation was performed with unimolecular dynamics results incorporated into the DSMC method. A comparison was performed between the total collision energy (TCE) model[5] of the DSMC method and the unimolecular dynamics approach by the use of different contributions of the relative translational energy to the energy of water dissociation. It was found that a physically reasonable level of 10% contribution of translational energy gave results similar to those of TCE with an OH vibrational temperature on the order of 2000 K. For a 100% contribution of translational energy, OH vibrational temperatures significantly higher than those predicted by traditional DSMC models were obtained. Therefore, the unimolecular dynamics approach suggested that the dissociation of water to produce OH could not be the mechanism that produced vibrtationally excited OH.

In subsequent work,[6] different chemical processes that might lead to vibrationally hot OH in the bow shock at high altitudes were investigated, and their effects on the overall vibrational temperature in the flow were estimated. The difficulties associated with modeling of the reactions leading to OH production were discussed along with

Received 14 April 2004; revision received 25 August 2004; accepted for publication 26 August 2004.

*Graduate Student, Department of Aerospace Engineering. 135 Hammond Building. Student Member AIAA.
†Associate Professor, Department of Aerospace Engineering, 233 Hammond Building; dalevin@psu.edu. Associate Fellow AIAA.
‡Research Assistant Professor, Department of Aerospace and Mechanical Engineering, 201 Rapp Research Building. Member AIAA.

the details of modeling of the postcollisional energy partitioning. An alternative to the conventional TCE model for water dissociation, based on a quasi-classical trajectory (QCT) treatment of the water dissociation by molecular nitrogen, was presented. The full QCT treatment validated the earlier approximate unimolecular calculations with the parameterized 10% contribution of translational energy assumption.

The four reaction mechanisms that may contribute to the total OH production were considered,[6]

$$H_2O + M \rightarrow OH + H + M \tag{1}$$

$$H_2O + O \rightarrow OH + OH \tag{2}$$

$$H + O_2 \rightarrow OH + O \tag{3}$$

$$O + H_2 \rightarrow OH + H \tag{4}$$

where $M = N_2$, O_2, and O. Process (1) represents the aforementioned water dissociation process, and processes (2–4) are the H_2O, O_2, and H_2 exchange reactions, respectively. In Ref. 6, it was found that using the TCE model for processes (3) and (4) may explain the higher OH vibrational temperature at 100 km. It was also observed that because the water dissociation is the dominant process at 80 km, the maximum OH vibrational temperature was about 2500 K.

Because of the potential importance of processes (3) and (4), it was decided to improve on the TCE model by use of a more exact, fundamental approach that uses the quasi-classical scattering approach to calculate the reaction cross sections. We then investigate the relative importance of different OH production reactions at two altitudes, 80 and 100 km, that will depend on the number densities of the chemical species and the reaction cross sections.

The goal of this work is to extend the quasi-classical treatment to the main exchange reactions for OH production and assess the influence of strong nonequilibrium between internal and translational modes on the reaction process as compared to the conventional TCE model used in DSMC. Finally, the results of the computations that elucidate the contribution of different reactions to the production of vibrationally hot OH are discussed.

II. QCT Calculations

The molecular dynamics (MD) method is known as quasi classical when quantum mechanical calculations are performed to determine the electronic potential energy surface (PES). The QCT/MD approach enables the physical investigation into chemical cross sections, reaction probabilities, and rate constants. Because these quantities depend on the motion of atomic nuclei, a classical rather than quantum treatment of that motion has been shown to provide a good approximation for the investigation of the reaction mechanisms. To perform QCT calculations, it is necessary to obtain an accurate PES for each reaction that reflects the changes in electronic energy as a function of internuclear distances.

As was mentioned, important mechanisms of OH production at high altitudes are the exchange reactions (3) and (4). A parallel MD code was developed and used to calculate the reaction cross sections for these reactions using the QCT–internal energy quantum mechanical threshold (QCT–IEQMT) method.[7] For reaction (3), a single-valued double many-body expansion potential energy surface for the ground state of HO_2, which is the transition state for reaction (3), is utilized.[8] Three particular features that make the QCT calculations for this reaction challenging are 1) that the PES has a deep well, 2) that the PES in the O + OH product arrangement channel is governed by a long-range dipole-induced quadruple interaction potential that is longer ranged than the usual interaction, and 3) that there are two heavy atoms involved in this reaction. For reaction (4), the London–Eyring–Polanyi–Sato potential of Johnson and Winter is utilized.[9]

A. Microcanonical Sampling

The multidimensional integrals associated with averaging scattering geometric properties before a collision are usually evaluated by an efficient Monte Carlo numerical procedure. The Monte Carlo method converges at a rate that is independent of the dimensionality of the integral. To utilize the Monte Carlo method, we need to specify the initial states of each of the trajectories so that it corresponds to the desired reaction probability. Microcanonical sampling enables one to sample the initial states of the target molecule of equal energy to perform the QCT calculations.[10]

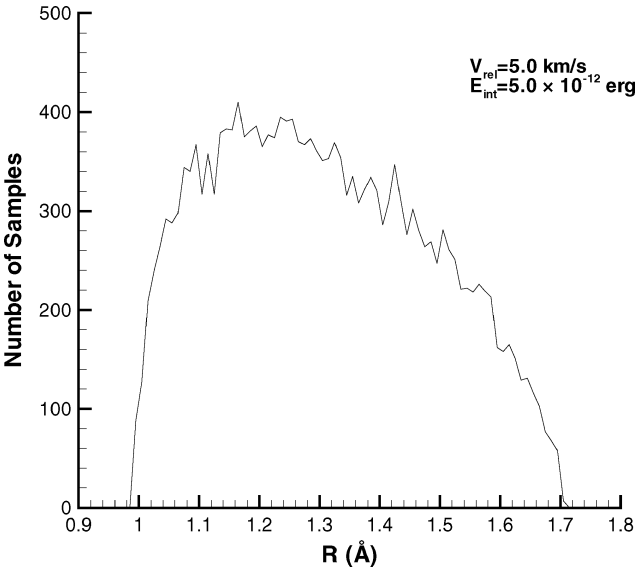

Fig. 1 State distribution of O_2 for reaction (3).

For the DSMC flowfield simulations, the probability of a chemical reaction as a function of translational energy E_{tr} and molecular internal energy E_{int}, obtained from the QCT calculations, will be used. Hence, we need to specify all possible precollisional coordinates and momenta that correspond to a specific value of E_{tr} and E_{int}. To select the Cartesian coordinates, we assume that the probability of selecting a diatomic molecule with a specific internuclear distance W is

$$W = [E_{int} - V(R_{12})]^{\frac{1}{2}} \tag{5}$$

where R_{12} is the O–O or H–H internuclear distance and E_{int} should be greater than the potential energy $V(R_{12})$. We allow the internuclear distance R_{12} to vary from R_{min} to R_{max}. R_{min} and R_{max} values should be selected so that the R_{min} is sufficiently smaller than the equilibrium internuclear distance R_{eq}, and the R_{max} is much larger than the R_{eq}. Once the maximum weighting factor W_{max} is determined, R_{12} is selected randomly as random number $RN \times R_{max}$, uniformly distributed from 0 to 1. The probability W/W_{max} is used in the standard acceptance–rejection technique to decide whether that value of R_{12} should be accepted as an initial condition. Figure 1 shows the distribution of the oxygen molecule with respect to internuclear distance, and, as expected, the distribution is at a maximum at the equilibrium internuclear distance.

In addition to the selection of precollisional molecule coordinates, the initial Cartesian momenta must be specified. This is accomplished by assuming that each Cartesian momentum coordinate has the form,

$$p_{i,j} = f RN_{i,j} \sqrt{m_j}, \qquad i = 1, 3, \qquad j = 1, 2 \tag{6}$$

where $RN_{i,j}$ represents six random numbers; i represents the index of x, y, and z; j is the index identifying the specific atom; and f is a proportionality constant that can be obtained by requiring conservation of energy.

B. Reaction Rate Constants

To verify the reliability of our QCT calculations, we need to compare the QCT calculations with published chemical rate data.

The thermal rate constant can be written as

$$k_f = f(T)Q_{\text{vib}}^{-1}Q_{\text{rot}}^{-1}\left(\frac{8kT}{\pi\mu}\right)^{\frac{1}{2}}\left(\frac{1}{kT}\right)^2 \times \sum_v\sum_J(2J+1)\int_0^\infty\int_0^{b_{\max}} P_r(v, J, E_{\text{tr}}, b) \times \exp\left(\frac{-E_{\text{tr}}}{kT}\right)2\pi b\,\mathrm{d}b E_{\text{tr}}\,\mathrm{d}E_{\text{tr}} \quad (7)$$

for reaction (3),

$$f(T) = \tfrac{1}{3} \quad (8)$$

and for reaction (4),

$$f(T) = \frac{5+\exp(-228/T)}{5+3\exp(-228/T)+\exp(-326/T)} \quad (9)$$

where $f(T)$ is the probability that the target molecular system is initially on an electronic surface that will allow a reaction to occur. For reaction (4), this function varies between 1 and $\frac{2}{3}$, changing from low to high temperature. To obtain the rate constant, the summations and integrals in Eq. (7) have been evaluated with the Monte Carlo method, as was discussed earlier.

At a given temperature, we define the reaction cross section by

$$\sigma_r(T) = \pi b_{\max}^2(N_r/N) \quad (10)$$

where N_r/N is the ratio of the number of reactive and total trajectories. The value of $b_{\max}$ is determined by trajectory calculations to be the largest impact parameter for which a reaction occurs. Reference 7 shows that, using a Monte Carlo approach in Eq. (7), one obtains the following expressions for the rate constants,

$$k_{f,3} = f(T)\left(\frac{8kT}{\pi\mu_{\text{H-O}_2}}\right)^{\frac{1}{2}}\sigma_r(T) \quad (11)$$

for reaction (3) and

$$k_{f,4} = f(T)\left(\frac{8kT}{\pi\mu_{\text{O-H}_2}}\right)^{\frac{1}{2}}\sigma_r(T) \quad (12)$$

for reaction (4). Figure 2 shows a comparison of the reaction rate constants, calculated using our parallel MD code at different temperatures, with the experimental data of Masten et al.[11] for reaction

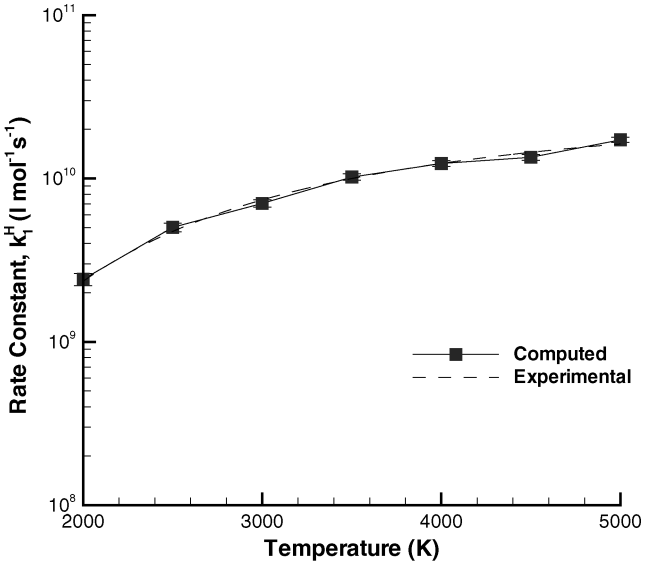

Fig. 2 Comparison of reaction rate constants for $H + O_2 \rightarrow OH + O$ reaction as a function of temperature.

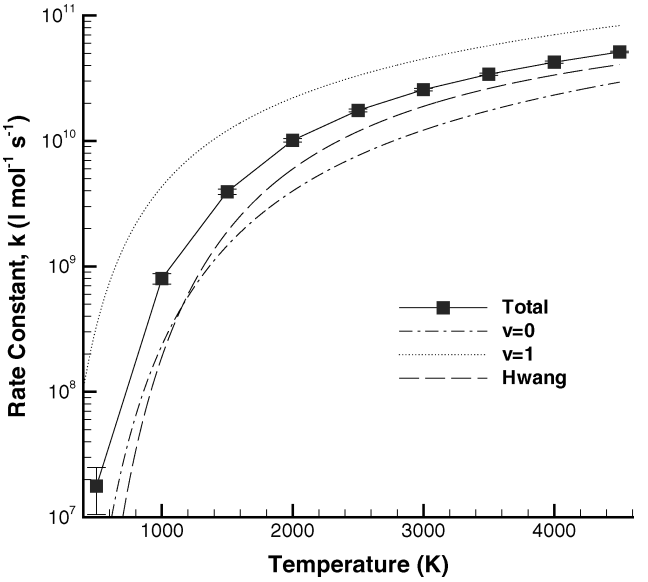

Fig. 3 Comparison of reaction rate constants for $O + H_2 \rightarrow OH + H$ reaction as a function of temperature (curves labeled "Total," "$v = 0$," and "$v = 1$" computed in this work).

(3). For reaction (4), Fig. 3 presents a comparison between the computed overall reaction rate constants, the reaction rate constants for the H_2 vibrational quantum numbers $v = 0$ and 1, and the experimental data of Hwang and Rabinowitz.[12] Note that the computed rates agree well with experimental values for reaction (3). For reaction (4), due to the high-temperature approximation for vibrational modes of H_2, the difference between the computed rates and the experimental data decreases as the temperature increases.

C. Comparison of TCE and MD Reaction Probabilities Used in DSMC

The reaction probability, the ratio of the reaction cross section obtained by the QCT–IEQMT method to the variable hard sphere (VHS) total collision cross section,[13] is used in the DSMC method to model the spatial distribution and temperatures of OH in the bow shock of a 5.1-km/s vehicle. The QCT reaction cross section is defined by

$$\sigma_r(E_{\text{tr}}, E_{\text{int}}) = \pi b_{\max}^2(N_r/N) \quad (13)$$

and is seen to depend on the translational and internal energies of the target molecule. The VHS model has a well-defined diameter and follows the classical hard sphere scattering law.[13]

The usual method for calculating the reaction probabilities in DSMC is the TCE model.[5] In this model, the reaction probabilities have a special form that allows one to match experimental reaction rates $K_f(T)$ in modified Arrhenius form,

$$K_f = AT^n\exp(-E_a/kT) \quad (14)$$

where A and n are constants and E_a is the activation energy.

Figures 4–6 show comparisons of reaction probabilities between the MD and TCE models as a function of internal energy for exchange reactions (3) and (4) and the $N_2 + H_2O$ dissociation reaction (1) at selected relative velocities, respectively. In the TCE model, all reactant internal energies were assumed to contribute to the reaction probability.

For the O_2 exchange reaction (3), the higher oxygen internal energies are needed for a reaction to occur. The MD reaction probability increases as the internal energy or relative translational energy increases. The reaction probabilities obtained by the TCE model increase rapidly at a collision energy equal to the activation energy E_a to a maximum value of about 0.2 for reaction (3). Note that in Fig. 4 the MD model is more sensitive to internal energies. One of the important features is that if the internal energy of the O_2 molecule is

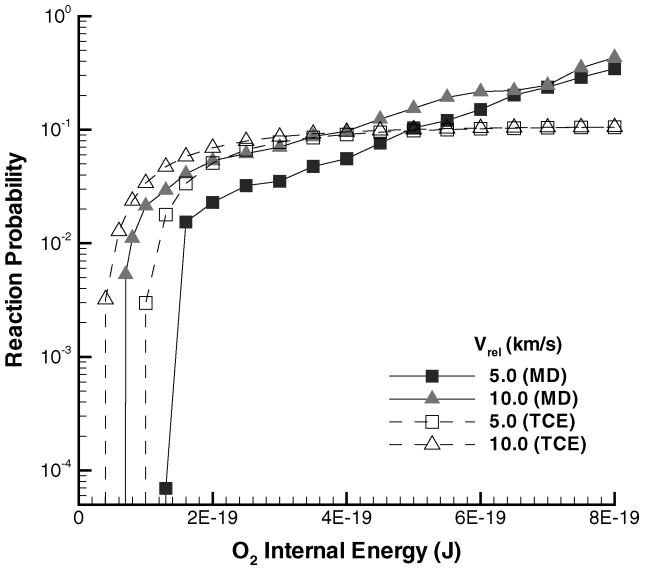

Fig. 4 Comparison between MD and TCE models; reaction probabilities for $H + O_2$ reaction as a function of oxygen internal energy at $V_{rel} = 5$ and 10 km/s.

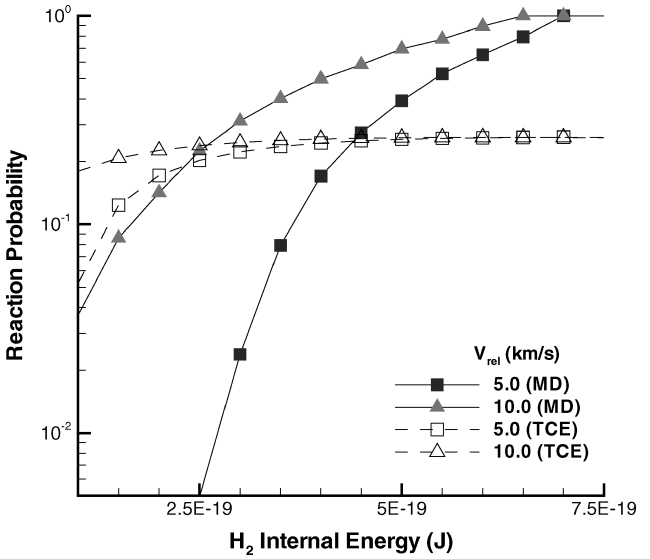

Fig. 5 Comparison between MD and TCE models; reaction probabilities for $O + H_2$ reaction as a function of hydrogen internal energy at $V_{rel} = 5$ and 10 km/s.

smaller than about 5×10^{-19} J, the MD reaction probability is lower than the TCE. Figure 5 shows that for reaction (4), the dependence of the MD reaction probability on the translational energy is more significant compared with reaction (3). The MD probability is seen to reach unity if the H_2 internal energy is higher than 6×10^{-19} J, which is a vibrational quantum number of approximately $v = 6$ or 7 (at $J = 1$). In contrast, the TCE reaction probabilities increase rapidly at a collision energy equal to the activation energy E_a to a maximum value of about 0.25 for reaction (4). For both exchange reactions, the TCE model probabilities are always higher than those of the MD model in the region, $V_{rel} = 3$–10 km/s, for small internal energy.

For the $N_2 + H_2O$ dissociation reaction (1), the probabilities obtained by both methods go to unity as the internal energy increases. Figure 6 shows that if the relative translational energy is small, the MD probabilities increase rapidly compared to those of TCE, and the MD probabilities can be higher than those of TCE. Also, the probabilities are sensitive to the relative translational energy in the region $V_{rel} = 3$–10 km/s and increase to unity.

Table 1 Rate constants for OH production reactions used in the TCE model

Reaction	A	n	E_a/k, K	Ref.
$H_2O + N_2 \rightarrow OH + H + N_2$	5.81×10^{-15}	0.00	−53,000	18
$H_2O + O_2 \rightarrow OH + H + O_2$	1.13×10^{-7}	−1.31	−59,400	18
$H_2O + O \rightarrow OH + H + O$	1.13×10^{-7}	−1.31	−59,400	18
$H_2O + O \rightarrow OH + OH$	1.13×10^{-16}	0.00	−9,240	18
$H + O_2 \rightarrow OH + O$	1.66×10^{-16}	0.00	−7,690	19
$O + H_2 \rightarrow OH + H$	3.12×10^{-16}	0.00	−6,897.5	12

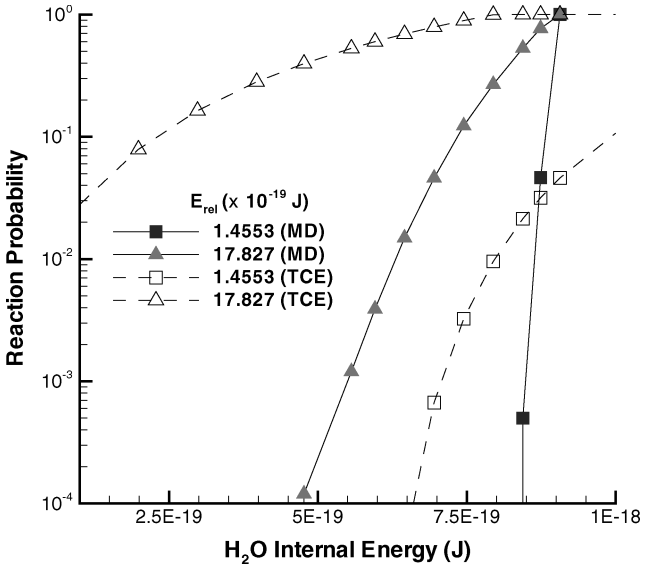

Fig. 6 Comparison between MD and TCE models; reaction probabilities for $N_2 + H_2O$ reaction as a function of internal energy at $E_{rel} = 1.4553 \times 10^{-19}$ and 17.827×10^{-19} J.

III. Numerical Flow Modeling Technique

The proposed computational approach is the DSMC method,[13] which is implemented in the SMILE computational tool. The SMILE capabilities include several different models for energy transfer, two-level rectangular grids adaptive to flow gradients, different grids for collisions and macroparameters, and the ability of efficient parallel computing implementation. The parameters for DSMC used were similar to those used by Gimelshein et al.[6] To minimize the statistical dependence between simulated particles, approximately 1,700,000 molecules were simulated in the computational domain. Separate grids were used for collisions and macroparameters adaptive to flow gradients. The total number of collision and macroparameter cells was 150,000 and 30,000, respectively. The total number of time steps was about 80,000 with a time step of 2.0×10^{-7} s for 80 km and 2.0×10^{-6} s for 100 km. Macroparameter sampling was started after 5000 time steps, a time sufficient to reach the steady state.

The majorant frequency scheme[14] is employed for modeling the molecular collision frequency, and the VHS model was used for modeling the interactions between particles. The discrete Borgnakke–Larsen[15] (BL) model (also see Refs. 16 and 17) with temperature-dependent rotational and vibrational relaxation numbers was chosen for modeling rotation–translation and vibration–translation energy transfer. The TCE and MD models were used to calculate the chemical reaction cross sections involving the chemical species N_2, O_2, H_2, H_2O, and their derivatives. The entire set of the chemical reactions can be found in earlier work,[6] and the hydrogenated reactions used in this work are presented in Table 1 (Refs. 12, 18, and 19).

The reactions in Table 1 have contributions to the OH production in the flows. The Arrhenius data presented in Table 1 were used to calculate the reaction cross sections based on the TCE model. The reaction cross sections for dissociation reaction (1), exchange reactions (3) and (4), were also calculated using the MD probabilities.

The OH and H_2O species were considered as trace species whose weighting factor was varied from 10^{-5} to 10^{-8} depending on the freestream concentrations of the trace species. In previous work,[6] it was found that the use of species weighting factors was important in reducing the statistical scatter of flow parameters related to trace species. The general idea is to increase the ratio of trace to major species concentrations to a value close to one. A full explanation of the computational procedure may be found in Ref. 20.

Two methods of postcollisional energy redistribution among reaction products were considered for those reactions modeled by the TCE. For dissociation, the Haas model of proportional decrease of mode energies was utilized.[21] Because this method cannot generally be applied for exchange reactions, the discrete BL model was used.

The gas–surface interaction was modeled using the Maxwell model. Three different accommodation coefficients were applied for translational, rotational, and vibrational modes of reflected molecules. The value of 0.85 was assumed for the translational accommodation coefficient, and a smaller value of 0.5 was selected for the internal energy accommodation coefficients.

IV. Results and Discussion

The discussion includes the general properties of the flow and a description of the impact of different OH production reactions on vibrational distributions and number densities. The calculations were performed for 80- and 100-km altitudes to study the reactive contribution of different OH production mechanisms using different chemistry models.

A. General Flowfield Features

Here we discuss the macroscopic parameters of the field. Note that the specific OH chemistry models do not affect the properties of major flow species, N_2, O_2, and O, so that the features of the major species are not sensitive to the OH production models. The computations were performed for a flow about a 0.2-m-diam sphere. The flow velocity is 5.1 km/s, the temperature of the sphere is 500 K, and the freestream conditions of reactants are given in Table 2.

Figure 7 shows the growth of the shock-layer width as the total density decreases. Figures 8 and 9 present the spatial distributions of the bulk translational, rotational, and vibrational temperature for 80- and 100-km altitudes along the stagnation line. The flow exhibits thermal nonequilibrium for both altitudes, as seen in Figs. 8 and 9. The degree of thermal nonequilibrium is higher for the 100-km altitude. A higher translational temperature is reached for altitude of 80 km with a magnitude about 14,000 K, and for 100 km the highest temperature is close to 11,000 K. All temperatures are higher at 80 km than they are at the corresponding values at 100 km. The translational temperature is an important property that determines the rates of chemical processes. The higher translational temperature at 80 km indicates that the relative collision velocities are higher for this altitude, and, hence, the reaction rates are higher for the TCE model. For the MD model the impact of the internal energy of the reactants plays a crucial role. Thus, the expected reaction rate is lower than for the TCE model. The degree of nonequilibrium between translational and internal modes is also an important factor for chemical reaction rates. For the 100-km altitude, the rotational and vibrational temperatures are much lower compared to the translational temperature; therefore, the translational mode contributes the most to the reaction cross sections.

Table 2 Freestream conditions

Condition	80 km	100 km
Total number density, m^{-3}	4.18×10^{20}	1.19×10^{19}
Temperature, K	185	181
O_2 mole fraction	0.21	0.18
N_2 mole fraction	0.79	0.78
H_2O mole fraction	5.6×10^{-6}	7.2×10^{-7}
OH mole fraction	4.3×10^{-9}	2.0×10^{-10}
O mole fraction	——	0.04
H mole fraction	5.0×10^{-8}	5.0×10^{-6}
H_2 mole fraction	5.3×10^{-7}	2.4×10^{-7}

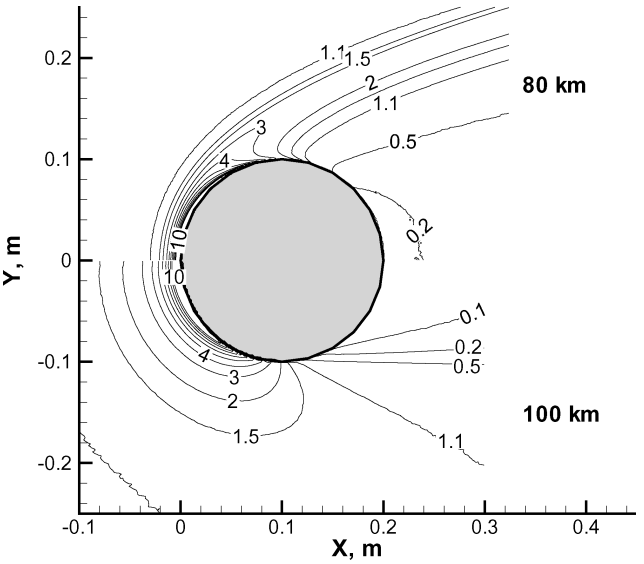

Fig. 7 Comparison of total number densities normalized by freestream values for 80 (top) and 100 km (bottom).

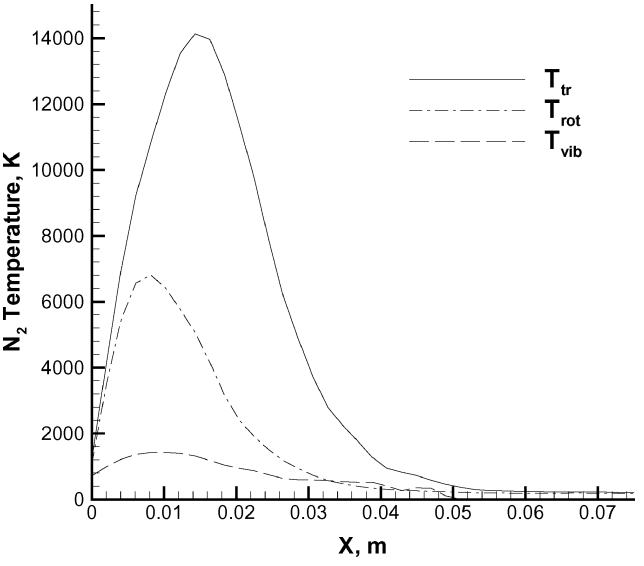

Fig. 8 N_2 temperature profiles along stagnation streamline for 80 km, wall located at $x = 0$ m.

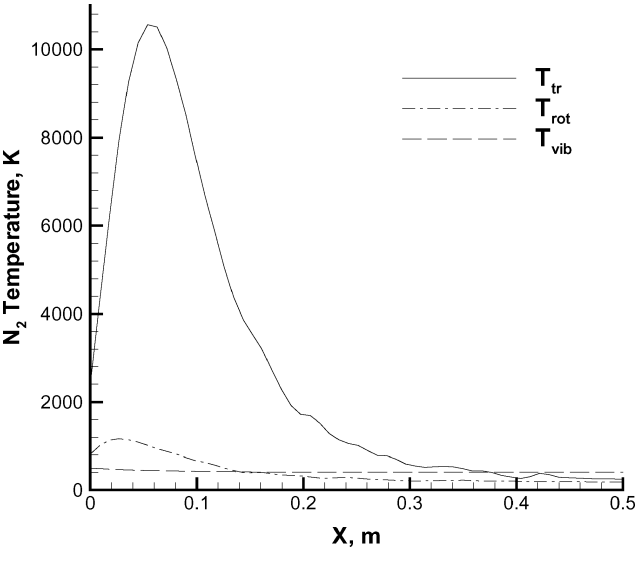

Fig. 9 N_2 temperature profiles along stagnation streamline for 100 km.

B. Contribution of Different OH Production Processes at 80 and 100 Kilometers

Figures 10 and 11 show the number density of OH for different reactions at 80 and 100 km, respectively, by the use of the TCE model. To study the relative contribution of the reactions, the DSMC computations were performed separately for each reaction. The normalized bulk curve shows the OH number density for the calculation excluding all OH production reactions, that is, the only source of OH is that from the freestream. In both cases, note that the chemical production of OH is important.

At 80 km, Fig. 10 shows that the water dissociation reaction (1) gives the greatest contribution to OH production. The water exchange reaction (2), which produces three times less OH near the body surface, starts later in the shock. This can be explained by the atomic oxygen (O) concentration in the flow. At 80 km, there is almost no O in the freestream, so that the reaction starts only after enough O is produced in the shock by oxygen dissociation. The next reaction $O + H_2$ (4) contributes about an order of magnitude less than the water exchange reaction and much less than dissociation. Similarly to water exchange, this reaction starts to contribute later in the shock. Although the $H + O_2$ reaction has almost no impact on the overall OH production because of the low freestream H concentration, it gives a higher number density than in the normalized bulk case.

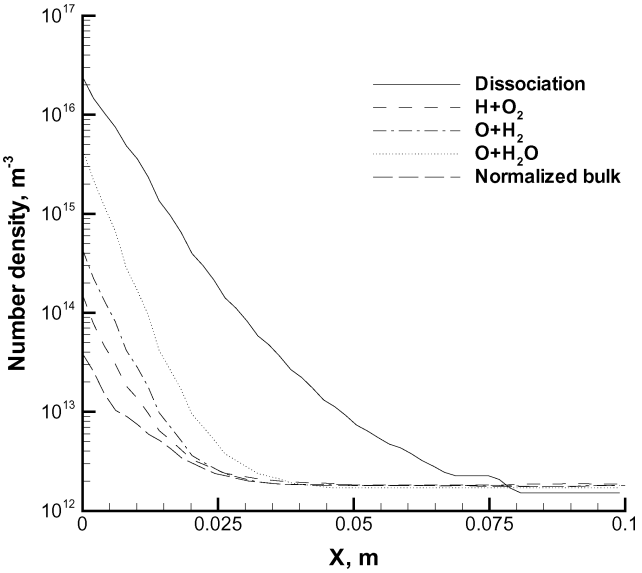

Fig. 10 OH number density along stagnation streamline at 80 km, contribution of different processes using TCE model.

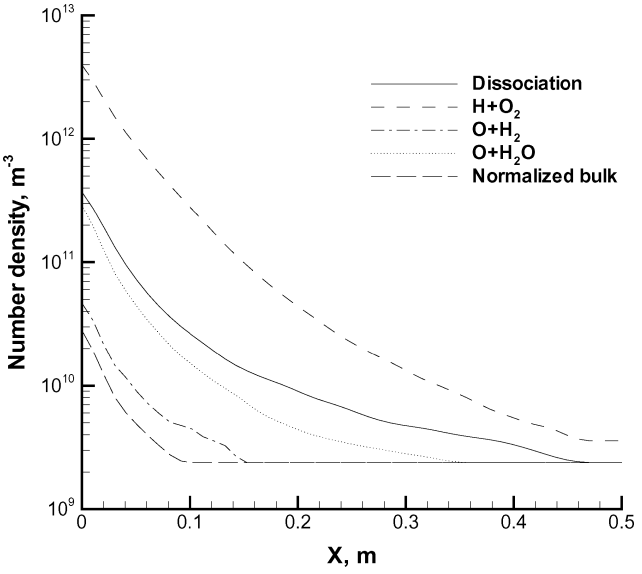

Fig. 11 OH number density along stagnation streamline at 100 km, contribution of different processes using TCE model.

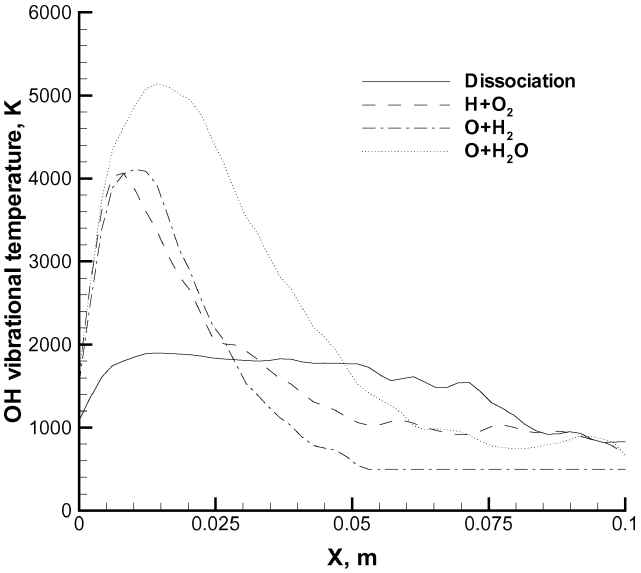

Fig. 12 OH vibrational temperature along stagnation streamline at 80 km, contribution of different processes using TCE model.

At 100 km, Fig. 11 shows that the order of importance changes. The most important reaction becomes the $H + O_2$ exchange reaction (3). The OH number density produced by this reaction at the body surface is about an order of magnitude larger than the number density of the second important reaction, water dissociation. The water exchange reaction gives a contribution similar to the dissociation, except that it starts later in the shock. For 100 km, the relative delay in a start of the water exchange reaction is less than for 80 km because the flow has more O in the freestream. Finally, the contribution of $O + H_2$ is about an order of magnitude less than the contributions from water dissociation and exchange and is close to the nonreaction case.

Whereas the relative contribution of water dissociation (1), exchange (2), and $O + H_2$ (4) reactions does not change for the two altitudes, the relative contribution of the $H + O_2$ reaction (3) changes significantly. This corresponds to the large difference in the freestream H mole fraction, 5.0×10^{-8} at 80 km and 5.0×10^{-6} at 100 km. Note that there is a significant uncertainty in the H and H_2 freestream concentrations at the altitudes under consideration.

Figure 12 presents profiles of OH vibrational temperature at 80 km for the four reactions. Water dissociation, the process that contributed the most OH at this altitude, gives the lowest vibrational temperature. The maximum vibrational temperature for the dissociation reaction is about 2000 K. The reason for such a low temperature compared to the other reactions is that a higher reaction heat is subtracted from the translational and internal energies of the reaction products. The highest OH vibrational temperature would be obtained by the $O + H_2O$ water exchange reaction (2) if it were the dominant production mechanism. This is mainly due to the contribution of three rotational and up to three vibrational modes of water that can be channeled into one vibrational mode of diatomic OH molecules, as well as that the internal energy mode excitation is significant at 80 km.

At 100 km, the OH vibrational temperature for the four reactions is presented in Fig. 13. All of the reactions give lower OH vibrational temperature than at 80 km due to the lower level of excitation of internal modes of the reactants at 100 km (Fig. 9). The OH vibrational temperature produced by the water dissociation reaction is much lower at 100 km than that at 80 km. This difference is due to the energy redistribution model used for the dissociation reaction. In the Haas redistribution model,[21] the OH internal energy is proportional to the H_2O internal energy, which is less for the 100-km altitude.

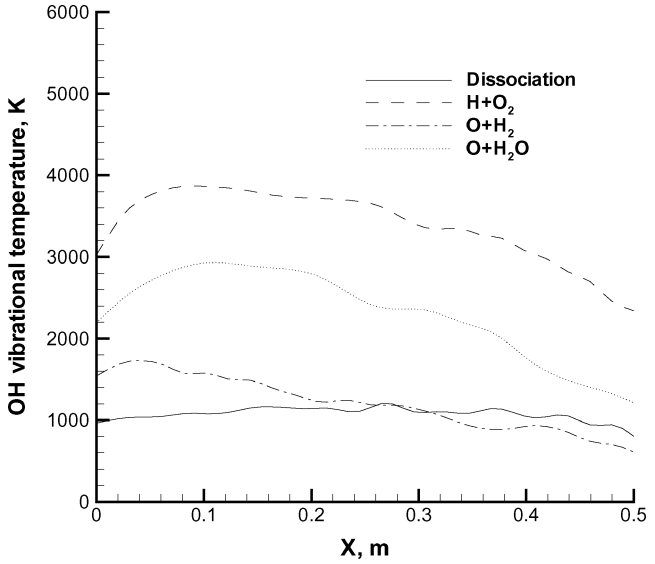

Fig. 13 OH vibrational temperature along stagnation streamline at 100 km, contribution of different processes using TCE model.

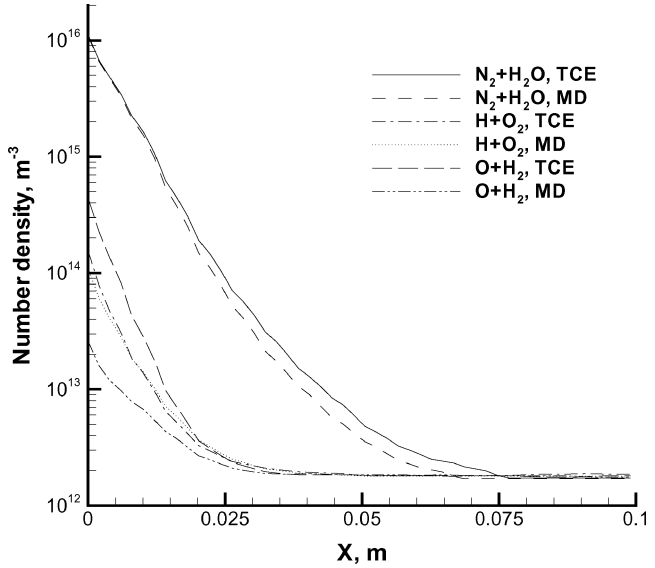

Fig. 14 OH number density along stagnation streamline at 80 km, comparison between MD and TCE models.

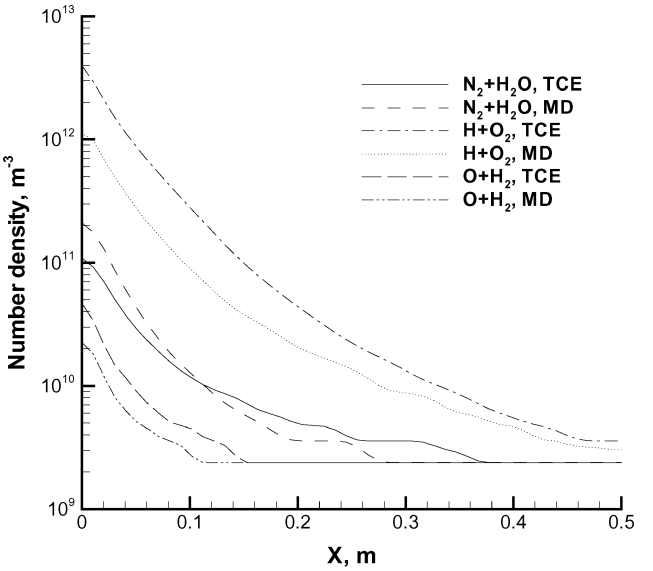

Fig. 15 OH number density along stagnation streamline at 100 km, comparison between MD and TCE models.

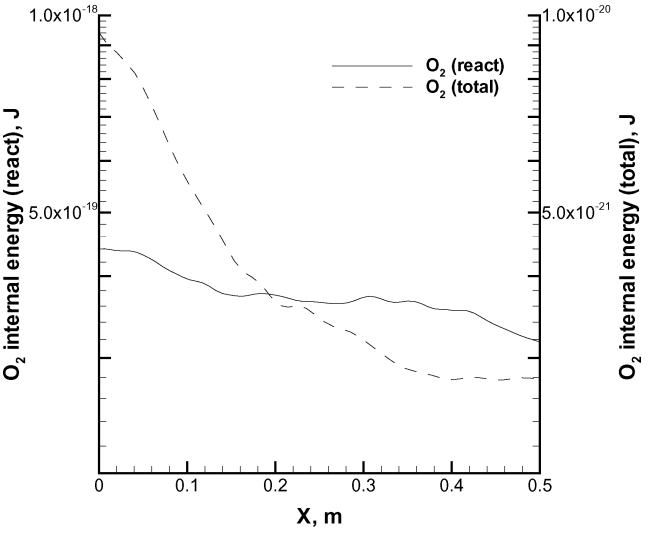

Fig. 16 Average internal energy of total O_2 molecules [O_2(total) with right *y* axis] and O_2 molecules that have reacted with H [O_2(react) with left *y* axis)] along stagnation streamline at 100 km using MD model, wall located at $x = 0$ m.

The highest vibrational temperature is observed for the $H + O_2$ reaction with a magnitude of about 4000 K, whereas the OH vibrational temperature produced by the $O + H_2$ reaction is the lowest. This may be explained in terms of the difference in reduced masses of the two sets of reactants[6] and that the fraction of cold freestream OH is greater for reaction (4) than for reaction (3).

C. Comparison Between the MD and TCE Chemistry Models at 80 and 100 Kilometers

Although the TCE model has been used as a standard DSMC chemistry model for over two decades, the accuracy of the model is questionable in highly nonequilibrium conditions. For systems where reliable potential energy surfaces exist, the MD model would be preferable because one can obtain reaction probabilities in highly nonequilibrium conditions for each specific energy mode. In this subsection, we compare the MD with the TCE model and evaluate the influence of strong nonequilibrium between internal and translational modes on the reaction process.

Figures 14 and 15 provide a comparison between the MD and the TCE models for OH number density along the stagnation streamline at 80 and 100 km for processes (1), (3), and (4). At both altitudes, the MD model produces less OH by the $O + H_2$ exchange reaction (4) because the MD reaction probability for this reaction is much lower than the TCE value when the H_2 molecules have small internal energy (Fig. 5). At 80 km, the main OH production reaction is the water dissociation. Therefore, although the MD and TCE reaction probabilities for reaction (4) do not agree, the overall OH production, as predicted by either the TCE or MD, agrees well.

In contrast, at 100 km, reaction (3) is the major OH production mechanism, and in this case there is a significant discrepancy between the TCE and the MD models. Figure 16 shows the average internal energy of all of the O_2 molecules compared to the average internal energy of only O_2 molecules that have reacted with H along the stagnation streamline at 100 km using the MD model. Figure 16 shows that the average precollisional internal energy of those O_2 molecules that have reacted with H is significantly higher than the average internal energy of all O_2 molecules. A comparison of these energies with reaction probabilities given in Fig. 4 shows that, for the internal energies in the stagnation region, the reaction (3) probability obtained by the MD model is lower than the TCE model. Therefore, because the MD model requires that the oxygen internal energy modes be excited before a reaction, the MD model

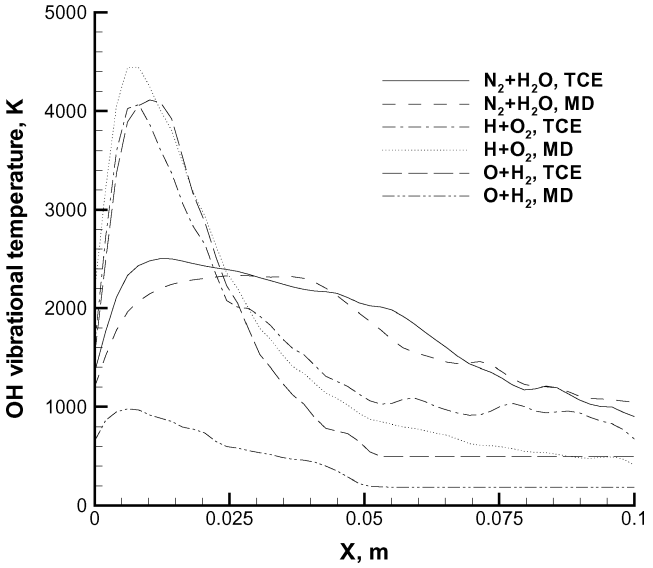

Fig. 17 OH vibrational temperature along stagnation streamline at 80 km, comparison between MD and TCE models.

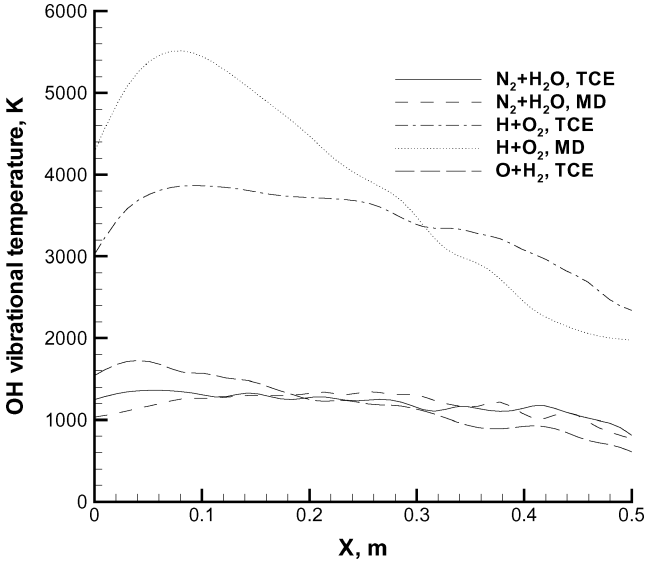

Fig. 18 OH vibrational temperature along stagnation streamline at 100 km, comparison between MD and TCE models.

manifests a significant delay in the OH number density increase at this altitude.

The OH vibrational temperatures for the three reactions at 80 and 100 km are given in Figs. 17 and 18, respectively. One of the important results is that the vibrational temperature of the $H + O_2$ exchange reaction (3) predicted by the MD model is higher than that by the TCE model. The result is more obvious at 100 km than 80 km, where the maximum vibrational temperature is over 5000 K. This behavior may be explained as follows. In the MD model, it is necessary to excite the internal energy modes to react with H, but after such collisions the higher internal energy forms OH molecules with excited internal energy modes. Moreover, the $H + O_2$ exchange reaction in the MD model shows a significant delay in the OH vibrational temperature increase. For oxygen molecules far from the body, which are in unexcited internal states due to low-temperature freestream conditions, the reaction rate is essentially zero in the MD model. For the $N_2 + H_2O$ dissociation reaction, the OH vibrational temperature obtained by the MD model agrees well with the TCE model at both altitudes. The last comparison is between the TCE and MD models for the $O + H_2$ exchange reaction (4), although this reaction has no significant influence on the overall OH vibrational temperature. Because the reaction rate derived with the MD model is much lower than that of the TCE model, the OH vibrational temperature produced by this reaction is only a little higher than the freestream temperature at both altitudes. For the MD model at 100 km, most of the OH molecules are in unexcited vibrational states due to the low reaction rate, thereby giving an OH vibrational temperature close to zero.

It is crucial to assess the OH vibrational populations for the modeling of the UV spectra of OH(A). As mentioned before, the characteristic that determines the ratio between the spectral maxima at 2800 and 3100 Å is the ratio of the OH(A) vibrational populations in the first and zeroth vibrational states. The population of OH(A) vibrational levels is assumed to be the same as that of OH. The assessment of this ratio based on the vibrational temperature can be inaccurate if the OH vibrational population is non-Boltzmann.

The normalized populations of vibrational levels 0–5 are shown in Figs. 19 and 20 for 80 and 100 km, respectively. The distributions may be approximated by two temperatures, one based on the first two vibrational levels and the other based on vibrational levels one and higher. At 80 km, the vibrational populations are non-Boltzmann for

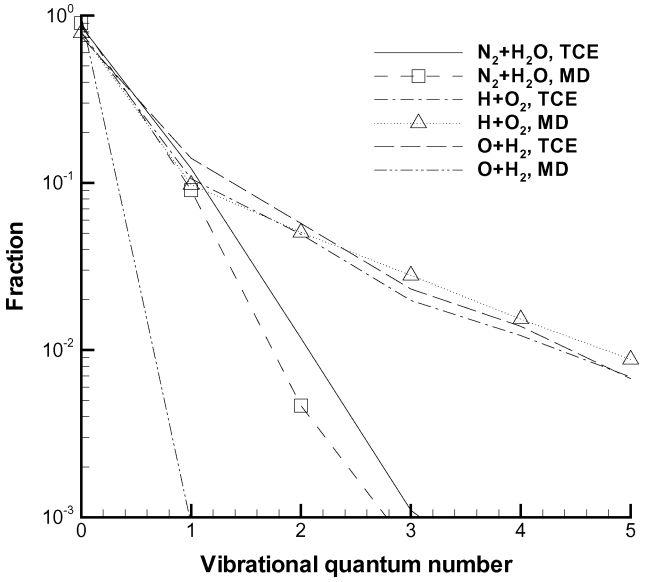

Fig. 19 OH vibrational distribution at 80 km shown at point of maximum vibrational temperature along stagnation streamline, comparison between MD and TCE models.

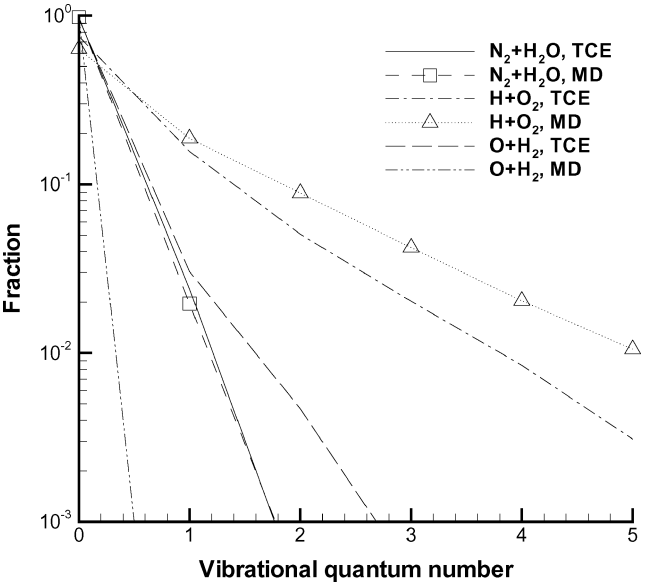

Fig. 20 OH vibrational distribution at 100 km shown at point of maximum vibrational temperature along stagnation streamline, comparison between MD and TCE models.

all three reactions (1), (3), and (4). The $H + O_2$ exchange reaction (3), which produces the highest OH vibrational temperature of the three reactions at both altitudes as shown earlier, predicts the highest vibrational product population for levels greater than two. At 80 km, the vibrational populations predicted by the TCE model for the $O + H_2$ exchange reaction (4) also predict OH vibrational levels similar to reaction (3). However, those predicted by the MD model are the lowest populations because of the low reaction rate and mixing with vibrationally cold OH from the freestream. At 100 km, all of the vibrational distributions are also non-Boltzmann, and as expected the vibrationally excited states are populated for the $H + O_2$ exchange reaction (3). This higher vibrational distribution of OH for reaction (3) in the MD model than the TCE model is consistent with the results of Fig. 18. These OH molecules populated in the vibrationally excited states are important for the overall result at 100 km because reaction (3) is the major OH production reaction at this altitude.

There are a number of reasons that explain the observed vibrational nonequilibrium: 1) The distributions of the translational and internal energies of the reactants are strongly nonequilibrium. 2) The subtraction of a large reaction heat in the dissociation reaction along with the proportional energy redistribution of the Haas model promotes an OH vibrational nonequilibrium distribution. 3) The OH molecules are a mixture of vibrationally cold OH molecules from the freestream. 4) One-half of the molecules reflected from the cool wall will have full internal energy accommodation. Most of the reflected molecules will be in the ground vibrational state, and some of them will penetrate upstream to the point of the highest vibrational temperature.

Finally, calculations were performed at 80 and 100 km to obtain OH number densities for two different complete reaction sets. The first set used only the TCE model for all air and hydrogenated reactions.[20] The second set substituted the MD reaction rates for reactions (1), (3), and (4); otherwise, the TCE model was used. At the 80-km altitude, the overall OH number density along the stagnation streamline of the MD model is nearly equal to that of the TCE model because OH production rates obtained by the TCE and MD for the major reaction, water dissociation, are about equal, as shown in Fig. 14. On the contrary, a significant discrepancy between two chemical reaction models is observed at the 100-km altitude. It is shown in Fig. 21 that the OH number density of the MD model is lower than that of the TCE model by a factor of three because the MD reaction probability for the $H + O_2$ exchange is lower than the TCE reaction probability for oxygen internal energy lower than 5.0×10^{-19} J. Although the reactant total energy increases due to collisions, the OH number density of the MD model may not be affected by the translational energy as much as the TCE model because the MD model is more sensitive to the reactant internal energies.

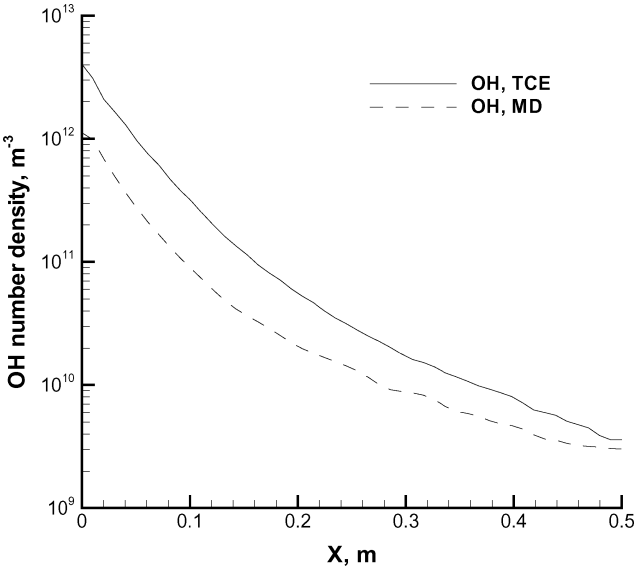

Fig. 21 Comparison of OH number density profiles along stagnation streamline at 100 km for TCE–BL and MD–BL models.

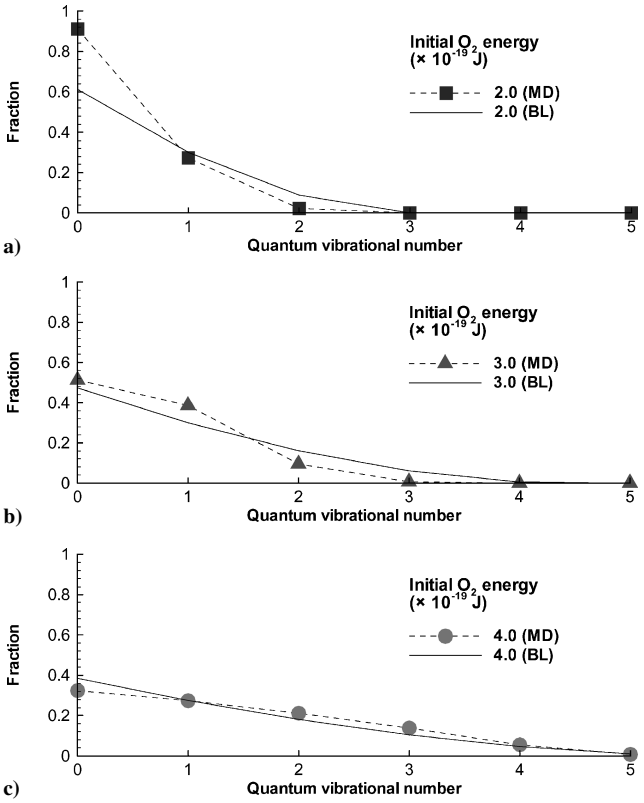

Fig. 22 Comparison of OH vibrational distributions for oxygen internal energies of a) 2×10^{-19} J, b) 3×10^{-19} J, and c) 4×10^{-19} J for reaction (3) between MD and BL models.

D. Comparison of OH Product Distributions Between the MD and BL Models

In this subsection, we compare the OH product vibrational distribution obtained by the QCT/MD method with the corresponding distribution of the BL model.[15] Figure 22 shows the comparison of OH product vibrational distributions between the MD and BL models for reaction (3), the main reaction at 100 km. The BL model predicts that more OH molecules are populated in excited vibrational states compared with the MD model for small O_2 internal energies. However, as the initial O_2 internal energy increases, the difference between the two models decreases. Figure 16 presented the average internal energy of O_2 molecules that have reacted with H atoms along the stagnation streamline at 100 km with the MD model. From Fig. 16, the average internal energy of O_2 molecules before the $H + O_2$ reaction is between 3×10^{-19} and 4×10^{-19} J. Figure 22 shows that in this range the MD model predicts similar OH product vibrational distribution to the BL model. This indicates that if one were to use the OH product vibrational distribution obtained by the MD model in the DSMC calculations, the high OH vibrational temperature at 100 km would be similar to the result of the BL product distribution energy model used in this work.

V. Conclusions

The DSMC method was applied to the calculation of the hypersonic flows about a sphere at 80 and 100 km. The objective of this work was to find the most important mechanisms for the production of vibrationally excited OH(A) observed in the BSUV2 experiment with the use of rigorous chemical reaction models. The TCE model was used to calculate reaction cross sections for all reactions. Furthermore, for three important reactions (1), (3), and (4), the reaction probabilities were obtained using the QCT/MD method to improve the fidelity of the chemical reaction models that could have important effects in nonequilibrium flows.

Four main processes that contribute to OH production in the flow were analyzed: water dissociation reaction (1), water exchange reaction with O reaction (2), and two exchange reactions between oxygen reaction (3) and hydrogen reaction (4).

The calculations show that at the 80-km altitude reaction (1) has the largest rate, but it predicts that OH will be formed with relatively low vibrational temperature. The other reactions that provide higher vibrational temperatures contribute less to OH number density. The OH vibrational temperature is higher at 80 km than that at 100 km due to higher excitation of the internal modes of the reactants.

At the 100-km altitude, the main OH production process is the $H + O_2$ exchange reaction (3). Moreover, this reaction gives the highest OH vibrational temperature in the shock wave. The MD model predicts slightly higher OH vibrational temperatures over 5000 K, compared to about 4000 K with the TCE model. This mechanism may explain the BSUV 2 spectral data and observation of the vibrationally hot spectra at the 100-km altitude. However, flight experiments that simultaneously measure spectral radiation and freestream conditions would provide a more definitive data set.

Acknowledgments

The research performed at the Pennsylvania Sate University was supported by U.S. Air Force Office of Scientific Research Grant F49620-02-1-0104, administered by Mitat Birkan, and U.S. Army Research Office Grant DAAD19-02-1-0196, administered by David Mann. Special thanks to Natalia Gimelshein for discussing the details of her calculations and Sergey Rogasinsky for his help with SMILE computational questions.

References

[1]Levin, D., Collins, R., Candler, G., Wright, M., and Erdman, P., "Examination of OH Ultraviolet Radiation from Shock-Heated Air," *Journal of Thermophysics and Heat Transfer*, Vol. 10, No. 2, 1996, pp. 200–208.

[2]Levin, D., Laux, C., and Kruger, C., "A General Model for the Spectral Calculation of OH Radiation in the Ultraviolet," *Journal of Quantitative Spectroscopy and Radiative Transport*, Vol. 61, No. 3, 1999, pp. 377–392.

[3]Kossi, K. K., and Boyd, I. D., "Detailed Computation of Ultraviolet Spectra in Rarefied Hypersonic Flow," *Journal of Spacecraft and Rockets*, Vol. 35, No. 5, 1998, pp. 653–659.

[4]Levin, D. A., Gimelshein, S. F., and Gimelshein, N. E., "Examination of Water Dissociation Models in Shock Heated Air," *Journal of Thermophysics and Heat Transfer*, Vol. 16, No. 2, 2000, pp. 251–260.

[5]Bird, G. A., "Monte Carlo Simulation in an Engineering Context," *Rarefied Gas Dynamics*, edited by S. Fisher, Vol. 74, Progress in Astronautics and Aeronautics, AIAA, New York, 1981, pp. 239–255.

[6]Gimelshein, N. E., Levin, D. A., and Gimelshein, S. F., "Hydroxyl Formation Mechanisms and Models in High-Altitude Hypersonic Flows," *AIAA Journal*, Vol. 41, No. 7, 2003, pp. 1323–1331.

[7]Varandas, A. J. C., Brando, J., and Pastrana, M. R., "Quasiclassical Trajectory Calculations of the Thermal Rate Coefficients for the Reactions $H(D) + O_2 \rightarrow OH(D) + O$ and $O + OH(D) \rightarrow O_2 + H(D)$ as a Function of Temperature," *Journal of Chemical Physics*, Vol. 96, No. 7, 1992, pp. 5137–5150.

[8]Pastrana, M. R., Quintales, L. A. M., Brandao, J., and Varandas, A. J. C., "Recalibration of a Single-Valued Double Many-Body Expansion Potential Energy Surface for Ground-State HO_2 and Dynamics Calculations for the $O + OH \rightarrow O_2 + H$ Reaction," *Journal of Physical Chemistry*, Vol. 94, No. 21, 1990, pp. 8073–8080.

[9]Johnson, B. R., and Winter, N. W., "Classical Trajectory Study of the Effect of Vibrational Energy on the Reaction of Molecular Hydrogen with Atomic Oxygen," *Journal of Chemical Physics*, Vol. 66, No. 9, 1977, pp. 4116–4120.

[10]Severin, E. S., Freasier, B. C., Hamer, N. D., Jolly, D. L., and Nordholm, S., "An Efficient Microcanonical Sampling Method," *Chemical Physics Letters*, Vol. 57, No. 1, 1978, pp. 117–120.

[11]Masten, D. A., Hanson, R. K., and Bowman, C. T., "Shock Tube Study of the Reaction $H + O_2 \rightarrow OH + O$ Using OH Laser Absorption," *Journal of Physical Chemistry*, Vol. 94, No. 18, 1990, pp. 7119–7128.

[12]Hwang, R. S., and Rabinowitz, M. J., "Rate Coefficient of the $O + H_2 \rightarrow OH + H$ Reaction Determined via Shock-Tube Laser Absorption Spectroscopy," *Chemical Physics Letters*, Vol. 242, No. 3, 1995, pp. 279–284.

[13]Bird, G. A., *Molecular Gas Dynamics and the Direct Simulation of Gas Flows*, Clarendon, Oxford, England, U.K., 1994, Chap. 2.

[14]Ivanov, M. S., and Rogasinsky, S. V., "Analysis of the Numerical Techniques of the Direct Simulation Monte Carlo Method in the Rarefied Gas Dynamics," *Soviet Journal of Numerical Analysis and Mathematical Modeling*, Vol. 3, No. 6, 1988, pp. 453–465.

[15]Borgnakke, C., and Larsen, P. S., "Statistical Collision Model for Monte Carlo Simulation of Polyatomic Gas Mixture," *Journal of Computational Physics*, Vol. 18, No. 4, 1975, pp. 405–420.

[16]Boyd, I. D., "Relaxation of Discrete Rotational Energy Distributions Using a Monte Carlo Method," *Physics of Fluids A*, Vol. 5, No. 9, 1993, pp. 2278–2286.

[17]Gimelshein, S. F., Boyd, I. D., and Ivanov, M. S., "Modeling of Internal Energy Transfer in Plume Flows of Polyatomic Molecules by the DSMC Method," AIAA Paper 99-0738, Jan. 1999.

[18]Baulch, D. L., Drysdale, D. D., Horne, D. G., and Lloyd, A. C., *Evaluated Kinetic Data for High Temperature Reactions*, Vol. 1, Butterworths, London, 1972, pp. 109–118, 349–355.

[19]Yang, H., Gardiner, W. C., Shin, K. S., and Fujii, N., "Shock Tube Study of the Rate Coefficient of $H + O_2 \rightarrow OH + O$," *Chemical Physics Letters*, Vol. 231, No. 4–6, 1994, pp. 449–453.

[20]Gimelshein, S. F., Levin, D. A., and Collins, R. J., "Modeling of Glow Radiation in the Rarefied Flow About an Orbiting Spacecraft," *Journal of Thermophysics and Heat Transfer*, Vol. 14, No. 4, 2000, pp. 471–479.

[21]Haas, B. L., "Modeling of Energy-Exchange Mechanics Applicable to a Particle Simulation of Reactive Flows," *Journal of Thermophysics and Heat Transfer*, Vol. 6, No. 2, 1992, pp. 200–207.